

## Thermographic investigation of the anisotropic behaviour of additively manufactured AISI316 steel using DED-Arc

by R. Krankenhagen\*, S. Chaudhuri\*, A. Pittner\*, R. Winterkorn\*, R. de Finis\*\*, D. Palumbo\*\*\*, U. Galietti\*\*\*

\* Bundesanstalt für Materialforschung und -prüfung, Unter den Eichen 87, 12205 Berlin, Germany  
*rainer.krankenhagen@bam.de*

\*\* University of Salento, Campus Ecotekne build O-S.P. 6, 73100 Lecce, Italy

\*\*\* DMMM-Politecnico di Bari, Via Edoardo Orabona 4, 70125 Bari, Italy

### Abstract

Additive manufacturing is one of the most promising techniques for industrial production and maintenance, but the specifics of the layered structure must be considered. The Direct Energy Deposition-Arc process enables relatively high deposition rates, which is favourable for larger components. For this study, specimens with different orientations were prepared from one AISI316 steel block – parallel and orthogonal to the deposition plane. Quasistatic tensile loading tests were carried out, monitored by an infrared camera. The obtained surface temperature maps revealed structural differences between both orientations. The consideration of surface temperature transients yields more details about the behaviour of the material under tensile loading than the conventional stress-strain-curve. These preliminary investigations were supplemented by thermographic fatigue trials. Although the anisotropy was also observed during fatigue loading the fatigue behaviour in general was the same, at least for both inspected specimens. The presented results demonstrate the abilities and the potential of thermographic techniques for tensile tests.

### 1. Introduction

The application of thermographic techniques is not limited to nondestructive testing and inspections but can also be used in connection with destructive methods. Typical cases are the investigation of crack growth [1, 2], the monitoring of impacts [3, 4], the investigation of the fatigue behaviour under cyclic loading [5] [6] and the determination of mechanical strength by static load trials [7]. These applications are based on the spatially and temporally resolved observation of surface temperature variation on object under test (OUT). Here, the thermoelastic effect in the elastic range [8] as well as the heat release from damaging processes in the plastic range [9] are in the focus of such investigations. Since both effects are directly related to the internal strain under loading the thermographic observation can provide valuable information about local strain distributions. These methods are often summarized under the name TSA (Thermoelastic Stress Analysis).

In this study, TSA was applied to analyse quasistatic load trials on AISI 316 steel additively manufactured by Direct Energy Deposition-Arc (DED-Arc), an additive process with relatively high deposition rates and specific pros and cons. A series of cross-section samples with different layer orientations was quasi-statically loaded until the ultimate stress level was reached. All trials were inspected with infrared thermography. Due to the large extension until final failure, the accurate evaluation of the surface temperature development in a certain region requires a reshape-procedure for the thermograms. In addition, individual specimens were exposed to cyclic loads with different amplitudes (step-based loading). The obtained thermographic results are discussed in relation to the stress-strain curves and a possible substructure of the material.

### 2. Sample preparation

DED-Arc is an additive manufacturing process that uses an electric arc to melt and deposit metal wire (equivalent to a weld pass) layer by layer, creating complex metal structures. This process enables faster deposition rates in comparison to powder-based materials [10].

A steel block measuring 250 x 40 x 150 mm<sup>3</sup>, made of AISI 316, was fabricated using a Direct Energy Deposition-Arc (DED-Arc) process. This setup included a 6-axis industrial robot, a Metal Inert Gas (MIG) power source, and additional sensors for monitoring the process. The manufacturing technique employed was the stringer-bead method. Each stringer bead, integral to the block's structure, was 40 mm long, matching the block's thickness. The design involved 39 layers, each comprising 55 stringer beads, totalling 2145 beads. A shielding gas mixture of 3% CO<sub>2</sub> in argon was used, flowing at a rate of 25 l/min. The deposition material chosen was a solid wire, G19 12 3 LSi (316LSi), in accordance with EN ISO 14343-A standard. A pulsed arc process was implemented for the deposition of all beads. Throughout the fabrication of all layers, the arc process parameters were consistently maintained at a wire feed rate of 6 m/min and a travel speed of 0.4

m/min. The entire manufacturing duration was approximately 12 hours, including time for interpass cooling to maintain a temperature below 100 °C. The finished block has a weight of 13.5 kg. Fig. 1 illustrates the layer deposition schematically.

Due to the layered build-up of the material, where every layer consists of parallel weld beads, anisotropic mechanical properties are expected. To investigate the anisotropy, tensile specimens of type E 2 x 16 x 40 according to DIN 50125 with different orientations were extracted. Here, the so-called ZPL and ZPS orientations are investigated; the cutting planes are indicated in Fig. 2. Both orientations cut the stringer beads in a plane, but the deposition physics behind is different. ZPL represents stringer beads deposited directly one after the other, while ZPS represents a deposition with a longer break between two stringer beads. In total, 7 specimens of both orientations were tested.

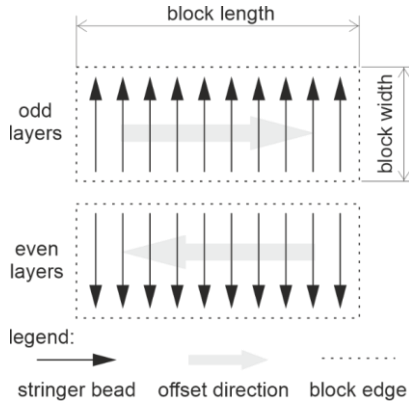


Fig. 1: deposition scheme of the individual layers, arrows indicate stringer beads

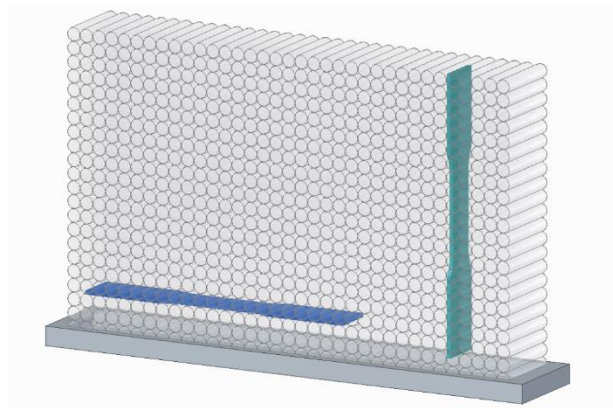


Fig. 2: Schematic of the primary bead structure of the print strategy, The blue specimen shows the ZPL orientation, the green specimen illustrates the ZPS orientation, a layered substructure is expected for both orientations

### 3. Experimental setup

The tensile tests were performed in accordance with DIN EN ISO 6892-1 using an MTS 810 testing machine, which provides a maximum test force of 25 kN. The testing speed was 0.025 mm/s. The setup is equipped with cameras and an illumination unit (see Fig. 3) to perform Digital Image correlation (DIC) measurements. The infrared inspections were realised by an infrared camera observing one surface of the respective specimen (also shown in Fig. 3).

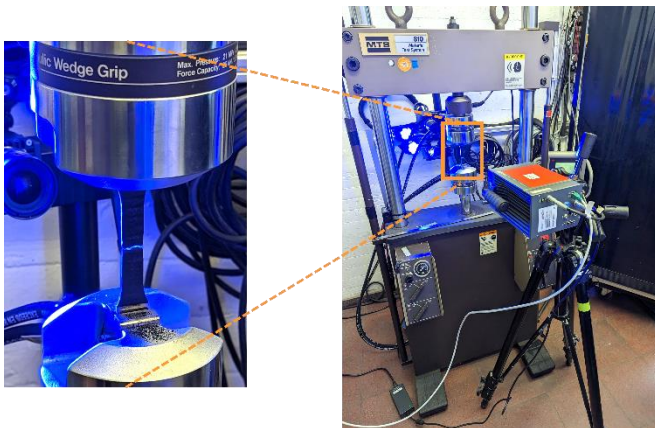


Fig. 3: setup for infrared observation during the quasi-static tensile test. The IR camera is in front (tilted by 90° to exploit the lateral extend of the detector array), the blue illumination is required for DIC measurements, the enlarged image displays the coated specimen and the clamps after ultimate failure

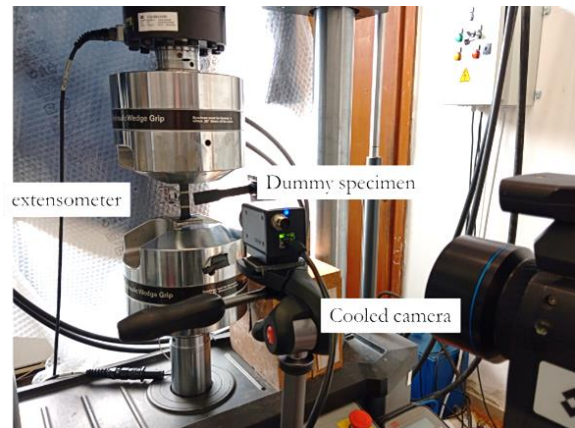


Fig. 4: setup for infrared observation during fatigue tensile test. The setup is similar but extended with a dummy specimen and a supplementary extensometer

The stress analysis during fatigue tests was performed with a different setup, which is shown in Fig. 4.. Fig. 4: setup for infrared observation during fatigue tensile test. The setup is similar but extended with a dummy specimen and a supplementary extensometer. The dummy specimen enables the observation of environmental influences on the thermographic results. The main camera parameters for both setups are compiled in Table 1:

**Table 1:** main camera parameters of the infrared cameras used for thermographic observations during quasi-static testing (first row) and during fatigue tests (second row).

Test	Detector	Pixel array	Frame-rate	Int. time	sequence length	Distance	Geometrical resolution
Quasi-static testing	Cooled MCT	320 x 240 (half frame format)	10 Hz	140 $\mu$ s	3...4 min (until fracture)	50 cm	3.3 pixel/mm
Fatigue testing	Cooled InAs	640 x 512	200 Hz	793 $\mu$ s	10 seconds	80 cm	6 pixel/mm

Please note that the quasi-static tensile tests comprise only one thermographic sequence per specimen while the fatigue tests always include three sequences for every selected loading level. Here, about 15 different loading levels with increasing amplitudes of fixed stress ratio equal to 0.1 by a cyclic frequency of 17 Hz were applied. More details of the general procedure are described in [11].

#### 4. Results from quasi-static tensile loads

In total, 7 ZPS specimens and 7 ZPL specimens were investigated. They were coated with HERP-LT-MWIR-BK-11 (manufactured by LabIR) on the front side to improve the thermographic results. This coating turned out to be flexible enough to endure 30 -35% strain. The effective emissivity was experimentally estimated to be >0.95 with the applied IR camera. The rear side was coated with a typical speckle pattern for the DIC measurements running in parallel during the trials.

The main outcome of the tensile tests is a stress vs. strain curve which allows the determination of typical material parameters such as elasticity modulus, the 0.2% offset yield strength, and the ultimate tensile strength. Fig. 5 demonstrates typical stress-strain curves for both orientations. Here, no specific difference could be observed between ZPS and ZPL specimens. Fig. 6 shows the appearance of two selected specimens after reaching the ultimate tensile load. In case of the ZPL-orientation a layered substructure appeared at the coated surface. In contrast, the surface of ZPS-specimen has an irregular deformed surface.

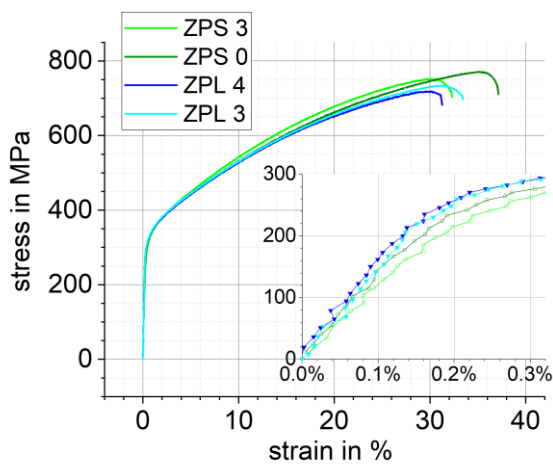


*Fig. 5: Stress-strain curves from two specimens of both orientations, stress values consider the real cross-section areas, the detail plot shows the results from low loading levels*

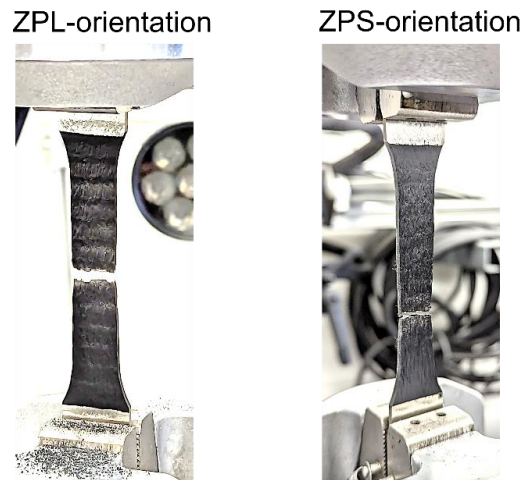


*Fig. 6: Enhanced photos from the specimens after ultimate failure, the ZPL specimen exhibits a layered surface structure, but not the ZPS specimen*

While the obtained mechanical material parameters are related to the central part of the specimen volume with constant cross section area, thermographic inspection as well as DIC provide full-field information about local heat release (thermography) and local deformations (DIC) during tensile stress. The next figures (Fig. 7 and Fig. 8) show thermograms of the specimens at different loading levels for both material orientations. The presented temperature values were obtained with the assumption that the emissivity is nearly 1.0 provided by the applied coating. The left-most thermogram in Fig. 7 and in Fig. 8 represents the initial temperature distribution before the loading has been started. The images to the right

represent different loading levels. In both cases the lower end was warmer probably due to conductive heating from the lower hydraulic clamp. Please note also the elongated specimen shape due to the high strain up to 30% resp. 35%. This prevents the consideration of difference thermograms to eliminate the influence of the inhomogeneous initial temperature distribution.

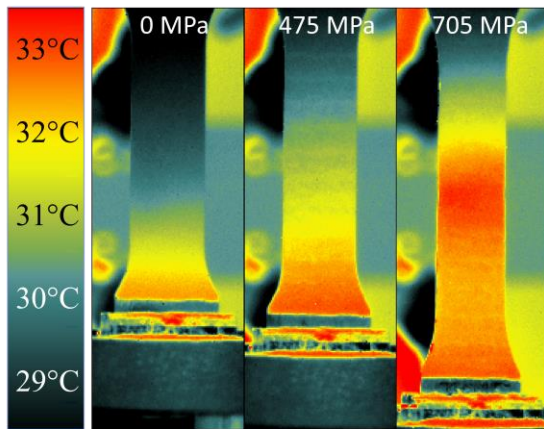


Fig. 7: Thermograms from the quasi-static tensile test on a ZPL-specimen at different loading levels: 0, 475 and 705 MPa

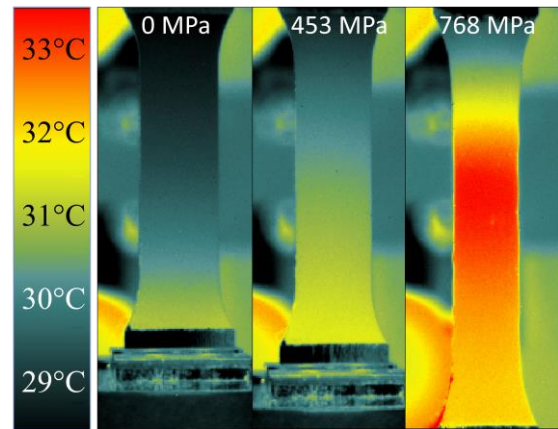


Fig. 8: Thermograms from the quasi-static tensile test on a ZPS-specimen at different loading levels: 0, 453 and 768 MPa

Here, the thermograms reveal different heating patterns for both orientations at lower loading levels (central image in Fig. 7 and Fig. 8). Thermograms of the ZPL specimen reveal a layered substructure, possibly related to the individual stringer beads. By contrast, the ZPS specimen showed a more homogenous temperature distribution. Both examples are typical for their respective orientation. The shape variation during the loading process prevents not only the calculation of difference thermograms but also the correct consideration of heat release and surface temperature transients like in [7]. This will be regarded in the discussion part.

## 5. Results from tensile fatigue testing

### 5.1 Thermoelastic Stress Analysis (TSA)

In thermographic fatigue investigations an instantaneous temperature distribution like in Fig. 7 and Fig. 8 only plays a minor role as demonstrated in other research [2, 11]. The average temperature does not permit a local analysis of the damage zone, as it only allows the detection of a larger region. Furthermore, the temperature is dependent on numerous factors, including heat exchange with the environment, which can result in difficulties in assessing damage areas. In these conditions it becomes difficult to detect thermal variations especially for those materials where the damage-related temperature changes are very small. Consequently, a more thorough filtering procedure is required. Thermoelastic Stress Analysis (TSA) is a well-established technique that allows to obtain information on material surface stress state by measuring the small temperature variations produced by cyclic loading in the elastic regime and adiabatic conditions (no thermal gradients related to the damage). The TSA technique is well-known to allow the identification of anomalies in the thermal map [11], which may be an indication of the presence of defects or manufacturing patterns in the material. In particular, temperature amplitude and phase lag variations are represented in Fig. 13 and Fig. 15 for sample ZPL0 and sample ZPS1, precisely revealing the differences between the two patterns. By comparing Fig. 13 and Fig. 15, both the temperature amplitude and the phase seems to be able to reveal the characteristic patterns induced by the technological process.

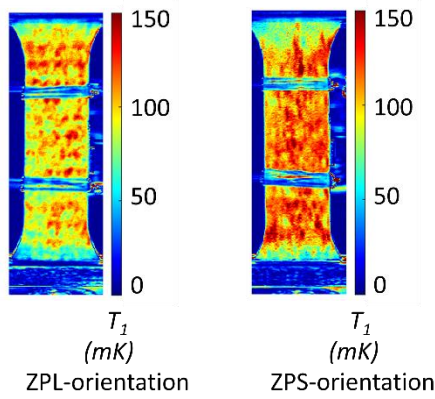


Fig. 9: Temperature amplitude maps for ZPL 0 and ZPS1 samples at a loading level in linear elastic condition (maximum stress 163 MPa)

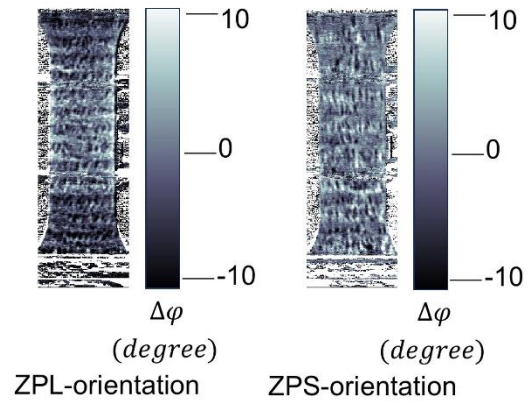


Fig. 10: Temperature phase lag maps for ZPL 0 and ZPS1 samples at a loading level in linear elastic condition (maximum stress 163 MPa)

## 5.2 Tensile fatigue testing

The analysis of thermoelastic temperature amplitudes and phase lags is also basis of the fatigue data evaluation. These parameters allow the observation of local phenomena, including zones of stress concentration [11] (amplitude maps) and zones of loss of adiabatic conditions [13] (phase maps), typical during damage processes.

It should be noted that the sample ZPL0 ruptured unexpected under medium load near the upper clamp, which was indicated before by a strong hot spot. Thus, the fatigue trial terminated at 163 MPa loading level.

The final result of a complete fatigue investigation is the compilation of amplitude and phase lag values for all loading levels, as shown in Fig. 11 and Fig. 12. Here, the entire region between the extensometer clips was used to calculate averaged values.

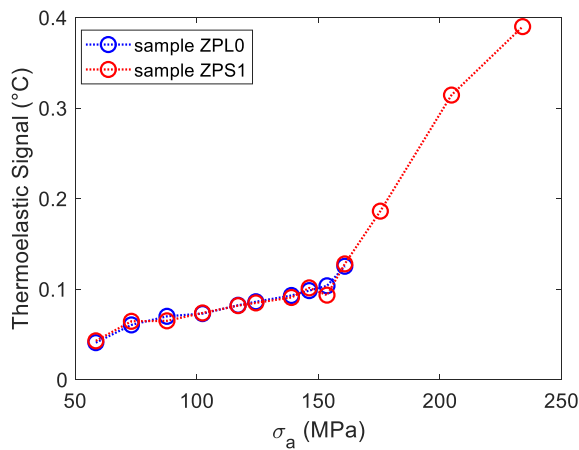


Fig. 11: Temperature amplitudes from the first harmonic for both samples ZPL 0 and ZPS 1 versus stress amplitude

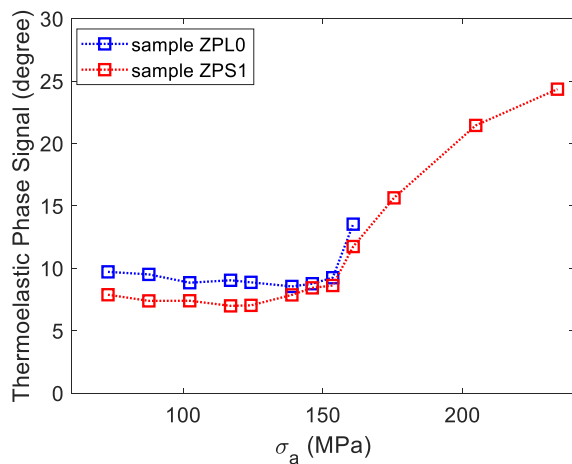


Fig. 12: Phase lags from the first harmonic for both samples ZPL 0 and ZPS 1 versus stress amplitude

From the analysis of the curves in Fig. 11 and Fig. 12 it can be seen, that there is a significant variation in both the thermoelastic amplitude as well as the phase around a stress amplitude of 150 MPa. The stress at which the significant variation of the thermal parameters is found can be considered as an estimator of the fatigue limit of the material, which seems to be in agreement with the results of previous studies [12].

Another noteworthy observation is that, despite the pronounced difference between the ZPL and ZPS specimens, there are no discernible differences in the fatigue behaviour of the two directions, at least from these preliminary investigations on these two specimens.

## 6. Discussion of quasistatic tensile testing

As described in the introduction part the heat release of a specimen under load is mainly determined by the local stress level. But the spatially resolved consideration of temperature transients could not be conducted in the usual way i.e. computing an average temperature within a selected region of interest (ROI) along the entire sequence. Therefore, a reshaping procedure was applied to compensate the shape variation due to the quasistatic loading tensile test. Essentially, the applied displacement on the test specimen due to the tensile tests was measured using object-tracking with the OpenCV Python library. Certain distinctive features in the testing machine grip that retained their appearance throughout the test were identified and tracked across all the images of a sequence. A transformation matrix based on the translation of the feature was used to perform the affine transformation (“warpAffine” function in OpenCV) on the thermograms to correct for testing machine actuator movement. The measured displacement is then used to produce a corrected thermogram where the original specimen size is kept, and the thermal data is representative of accumulating plastic deformation.

The results of the reshaping procedure are exemplarily presented in Fig. 13, for the ZPL specimen. All significant thermographic features remained. But now, difference thermograms can be calculated (Fig. 14). This procedure suppresses the influence of the heat impact from the lower clamp and makes the heat release due to damaging processes in the central part more distinguishable.

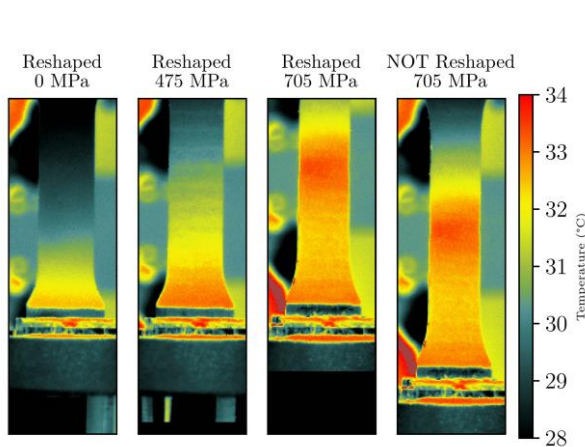


Fig. 13: Corrected thermograms from the quasi-static tensile test on a ZPL-specimen at different loading levels: 0, 475 and 705 MPa compared with the “un”-corrected thermogram.

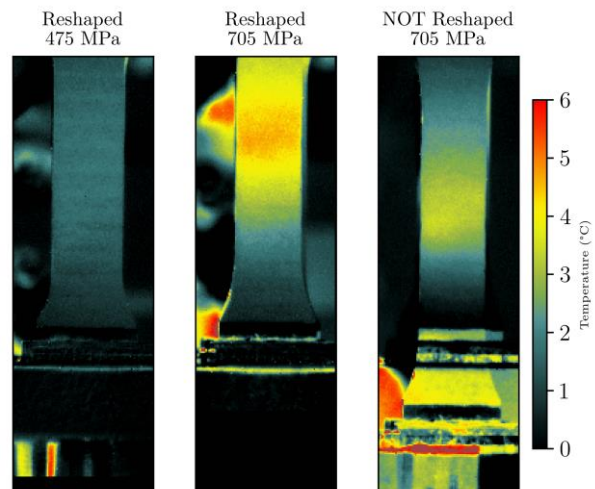


Fig. 14: Difference thermograms of two corrected thermograms from Fig. 13 with the first thermogram of the trial, a difference thermogram of raw data is shown separately on the right side (discussion in text)

This can easily be verified by the furthest to the right difference thermogram in Fig. 14 which represent a difference thermogram without reshaping. The modified stretched sample geometry results in “ghost” features in the lower part, and the maximum temperature in the central region is certainly lower than in the corrected difference thermogram. This results probably from the incorrect difference calculation with a “zero-thermogram” with a lower warm clamp. Thus, raw thermograms strongly suffered by the initial inhomogeneous temperature distribution of the specimens. A similar issue was also regarded in [13] for fatigue measurements.

The obtained sequences of difference temperature distributions allow the quantitative analysis of the layered substructure of the ZPL specimen detected at the raw thermograms (see Fig. 7). To highlight the wavy substructure some profile lines in vertical direction were averaged to reduce the noise influence. Fig. 15 and Fig. 16 show the results for ZPL and ZPS orientation providing again the different behaviour of material orientations under tensile loading. The temperature profiles from the lowest tensile load are well below the yield strength, thus they are representing the thermoelastic cooling effect. Please note the rising of the wavy substructure at the ZPL orientation starting in the range of 400 ... 500 MPa tensile load. This appeared in parallel to the general temperature increase with its maximum in the central part of the specimen with the smallest cross-section area. The amplitude of the temperature substructure is about 200 mK between minimum and maximum, with a spatial width of about 18 pixels., which is equivalent to 5.5 mm. This value is 10% higher than expected from the original width of 4.5 mm per bead with additional 10% strain for 500 MPa. Perhaps it is an indication of inhomogeneous strain distribution along the vertical axis.

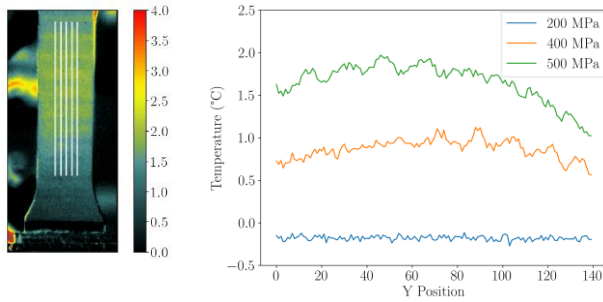


Fig. 15: averaged difference temperature profile lines from a ZPL-specimen under different loading levels, each profile is an average of 5 individual parallel profile lines indicated in the thermogram on the left side

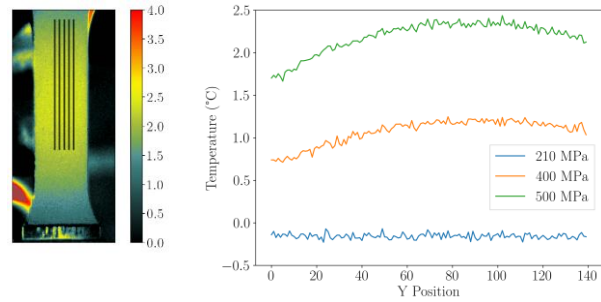


Fig. 16: averaged difference temperature profile lines from a ZPS-specimen under different loading levels, each profile is an average of 5 individual parallel profile lines indicated in the thermogram on the left side

Reshaped thermograms also allow the consideration of surface temperature transients within stationary regions of interest (ROI). However, using a large ROI (large means large in comparison to the entire strain of the specimen) the general shape of the transient curve is not really influenced by the reshaping. This can be inspected on Fig. 17, where the stress curve is also plotted for comparison. The most impressive feature of this comparison is that the temperature curves have a lot of features while the stress-strain curve is almost featureless although the same process was monitored. One interesting aspect is the appearance of a plateau between 5 and 18% strain. From a physical point of view, it indicates a change of the internal deformation processes within this strain range to other processes with almost no heat release. During further strain increase a second change appeared, back to the usual behaviour with heat release. The transition is sharp like an internal phase transition. On the other hand, the usually observed stress-strain-curve shows no indication of these internal changes at all. The transients of the ZPS specimens (not shown here) also reveal a series of temporal peaks but not this plateau.

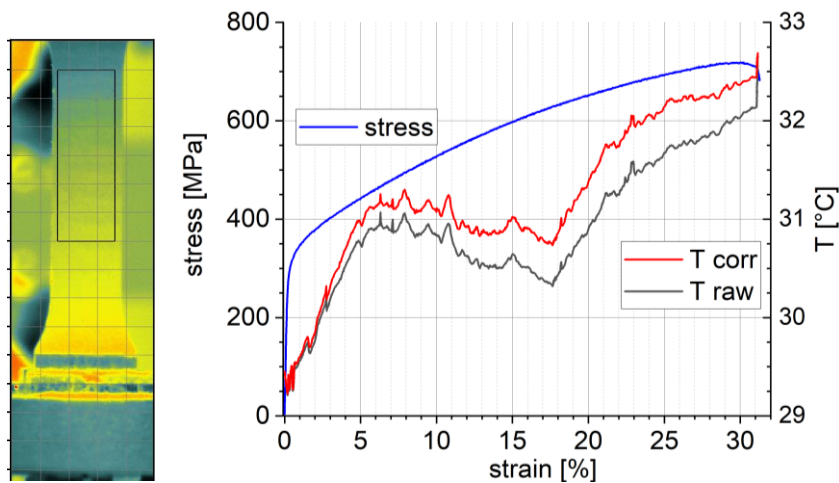


Fig. 17 comparison of a raw temperature and a corrected (by reshaping) temperature transient profile (right scale) of the ZPL-specimen, averaged within the ROI indicated in the thermogram on the left side, the related stress-strain curve (left scale) was already shown in Fig. 5

All presented thermographic results were obtained at one ZPL specimen and one ZPS specimen. Further results from other specimens are similar but could not be reported here. The next step will be a complete evaluation of the entire data sets from both: the mechanical as well as the thermographic investigations. In case of fatigue testing only the two presented data sets were available, but further trials are scheduled. Of course, the assumptions and explanations concerning the substructure must be verified by further investigations including DIC and optical micrography. Further, it is necessary to investigate the other orientations of the manufactured block to understand the general behaviour of this kind of material.

## 7. Conclusions

Specimens of two different orientations were machined from an AISI 316 L block manufactured by DED-arc. The different samples were investigated in tensile loading: quasi-static until ultimate failure and cyclic with different loading levels to characterize the fatigue behaviour. Both methods were assisted by thermographic observations to learn more

about the spatial distributions of stress and damaging processes. The thermographic results were similar across quasi-static and fatigue loading. The specimens of one orientation (ZPL) reveal a substructure noticeably related to the manufacturing process. In order to correct the strong deformation due to a strain of 30% and more the thermographic sequences were processed with image processing tools to achieve a reshaping. A direct comparison of conventional stress-strain curves with temperature strain curves could demonstrate the sensitivity of the temperature signal to inner structural changes without any equivalent indication in the stress strain curve. In case of the ZPL orientation, a plateau appeared in the temperature strain curve related to strain processes with almost no heat release far beyond the yield strength. Although some mechanisms and their thermographic signature are not yet fully understood, the obtained results highlight the additional benefits of using thermographic observations in conventional material investigations.

### References

- [1] R.A. Tomlinson, E.A. Patterson, Examination of Crack Tip Plasticity Using Thermoelastic Stress Analysis, in: T. Proulx (Ed.) *Thermomechanics and Infra-Red Imaging*, Volume 7, Springer New York, New York, NY, 2011, pp. 123-129.
- [2] F. Ancona, R. De Finis, D. Palumbo, U. Galietti, Crack Growth Monitoring in Stainless Steels by Means of TSA Technique, *Procedia Engineering* 109 (2015) 89-96.
- [3] C. Meola, G.M. Carlomagno, Infrared thermography to evaluate impact damage in glass/epoxy with manufacturing defects, *Int J Impact Eng* 67 (2014) 1-11.
- [4] C. Maierhofer, R. Krankenhagen, M. Röllig, Application of thermographic testing for the characterization of impact damage during and after impact load, *Compos Part B-Eng* 173 (2019).
- [5] J.C. Krapez, D. Pacou, G. Gardette, Lock-in thermography and fatigue limit of metals, *Conference proceedings QIRT 20000* (2000) 6.
- [6] A. Risitano, G. Risitano, Determining fatigue limits with thermal analysis of static traction tests, *Fatigue & Fracture of Engineering Materials & Structures* 36(7) (2013) 631-639.
- [7] F. Libonati, L. Vergani, Damage assessment of composite materials by means of thermographic analyses, *Compos Part B-Eng* 50 (2013) 82-90.
- [8] J.M. Dulieu-Barton, P. Stanley, Development and applications of thermoelastic stress analysis, *The Journal of Strain Analysis for Engineering Design* 33(2) (1998) 93-104.
- [9] N.F. Enke, An enhanced theory for thermographic stress analysis of isotropic materials, *Stress and Vibration: Recent Developments in Industrial Measurement and Analysis*, SPIE, 1989, pp. 84-102.
- [10] K. Treutler, V. Wesling, The Current State of Research of Wire Arc Additive Manufacturing (WAAM): A Review, *Applied Sciences* 11(18) (2021) 8619.
- [11] R. De Finis, D. Palumbo, U. Galietti, A multianalysis thermography-based approach for fatigue and damage investigations of ASTM A182 F6NM steel at two stress ratios, *Fatigue & Fracture of Engineering Materials & Structures* 42(1) (2019) 267-283.
- [12] A. Avanzini, Fatigue Behavior of Additively Manufactured Stainless Steel 316L, *Materials* 16(1) (2023) 65.
- [13] R. De Finis, D. Palumbo, F. Ancona, U. Galietti, Fatigue limit evaluation of various martensitic stainless steels with new robust thermographic data analysis, *International Journal of Fatigue* 74 (2015) 88-96.